© 2017. Published by The Company of Biologists Ltd | Journal of Cell Science (2017) 130, 879-891 doi:10.1242/jcs.199117

RESEARCH ARTICLE

IFT57 stabilizes the assembled intraflagellar transport complex and mediates transport of motility-related flagellar cargo

Xue Jiang, Daniel Hernandez, Catherine Hernandez, Zhaolan Ding, Beiyan Nan, Karl Aufderheide and Hongmin Qin*

ABSTRACT

Intraflagellar transport (IFT) is essential for the assembly and maintenance of flagella and cilia. Recent biochemical studies have shown that IFT complex B (IFT-B) is comprised of two subcomplexes, IFT-B1 and IFT-B2. The IFT-B2 subunit IFT57 lies at the interface between IFT-B1 and IFT-B2. Here, using a *Chlamydomonas reinhardtii* mutant for IFT57, we tested whether IFT57 is required for IFT-B complex assembly by bridging IFT-B1 and IFT-B2 together. In the *ift57-1* mutant, levels of IFT57 and other IFT-B proteins were greatly reduced at the whole-cell level. However, strikingly, in the protease-free flagellar compartment, while the level of IFT57 was reduced, the levels of other IFT particle proteins were not concomitantly reduced but were present at the wild-type level. The IFT movement of the IFT57-deficient IFT particles was also unchanged. Moreover, IFT57 depletion disrupted the flagellar waveform, leading to cell swimming defects. Analysis of the mutant flagellar protein composition showed that certain axonemal proteins were altered. Taken together, these findings suggest that IFT57 does not play an essential structural role in the IFT particle complex but rather functions to prevent it from degradation. Additionally, IFT57 is involved in transporting specific motility-related proteins.

KEY WORDS: Cilia, Flagella, IFT particles, IFT complex, Flagellar assembly, IFT57, Flagellar motility

INTRODUCTION

Eukaryotic cilia and flagella project from the surface of almost all interphase cells where they perform a variety of signaling and motility-based functions (Ishikawa and Marshall, 2011). The assembly and function of the cilium rely on intraflagellar transport (IFT), which is a bi-directional traffic of linear trains of IFT particles along the axoneme (Pigino et al., 2009). Ciliary defects, including those caused by IFT deficiencies, are linked to ciliopathies, such as polycystic kidney disease (PKD) and Bardet–Biedl syndrome (BBS) (Badano et al., 2006).

The IFT particle is comprised of two biochemical separable complexes, IFT-A and IFT-B, which contain six and 16 subunits, respectively (Ishikawa and Marshall, 2011). Research in the past decade has made great advances into determining the architecture of the IFT complexes, especially the IFT-B complex (Behal et al., 2012; Taschner et al., 2016; Katoh et al., 2016). The IFT-B complex contains a salt-resistant core complex and several peripheral proteins (Lucker et al., 2005). An earlier yeast two-hybrid assay shows that the peripheral proteins IFT57 and IFT20 directly interact (Baker et al., 2003), providing the first clue that the peripheral proteins may not just loosely stick onto the IFT-B core complex, but rather form complexes. Indeed, two very recent comprehensive mappings of interactions among all IFT-B subunits demonstrate that all peripheral proteins [IFT20, IFT54 (also known as TRAF3IP1), DYF-3 (also known as Cluap1), IFT57, IFT80 and IFT172] form a distinct biochemical complex which is now called IFT-B2. The core complex, containing IFT22, IFT25 (also known as HSPB11), IFT27, IFT46, IFT52 (also known as BLD1), IFT56 (also known as TTC26 and DYF-13), IFT70 (also known as DYF-1), IFT74, IFT81 and IFT88, is renamed as IFT-B1 (Katoh et al., 2016; Taschner et al., 2016).

Several subunits play prominent roles in IFT-B assembly. IFT52 is the backbone for the IFT-B1 subcomplex IFT88–IFT70–IFT52–IFT46 (Taschner et al., 2011; Richey and Qin, 2012). IFT52 is also essential for the overall stability of IFT-B1 because it mediates the binding of the subcomplex IFT88–IFT70–IFT52–IFT46 with the other subcomplex IFT81–IFT74–IFT27–IFT25–IFT22 (Taschner et al., 2014, 2011). Recently, the Lorentzen and the Nakayama laboratories, using expressed *Chlamydomonas reinhardtii*, and human or mouse proteins, respectively, have biochemically mapped the subunits at the interface between IFT-B1 and IFT-B2 (Taschner et al., 2016; Katoh et al., 2016). IFT57 and DYF-3 in IFT-B2, and IFT52 and IFT88 in IFT-B1 are the proteins that bridge the two subcomplexes together to form a complete IFT-B complex. Consistent with this, in *Chlamydomonas*, the IFT-B complex completely fails to assemble in the *ift52* mutant, while IFT-B2 proteins dissociate from the IFT-B1 complex in the *ift88* mutant (Richey and Qin, 2012). The essential role of DYF-3 in IFT-B assembly has also been verified by the cultured *Cluap1*$^{-/-}$ MEF cell line (Katoh et al., 2016). Currently, among the four interface subunits, only the impact of IFT57 on the *in vivo* assembly of the IFT-B complex has not been examined.

It is unknown whether individual subunits of IFT57 and DYF-3 are sufficient for the interaction with IFT88–IFT52, the interface of IFT-B1. The Nakayama group, through the use of visible immunoprecipitation (VIP) assays, has shown that IFT57 and DYF-3 are important for mediating the binding between the two IFT-B subcomplexes (Katoh et al., 2016). However, since IFT57 and DYF-3 could only be purified as a single complex, whether individual subunits or both are necessary for the interaction with IFT88–IFT52 still needs to be determined (Taschner et al., 2016). Moreover, the work from the Lorentzen group uses purified proteins from *E. coli* (Taschner et al., 2016), while the interaction mapped by Nakayama and colleagues has been analyzed through exploration of an artificial overexpression system (Katoh et al., 2016). Ideally, the role of IFT proteins in IFT complex assembly should be addressed in an organism with a functional IFT.

Department of Biology, Texas A&M University, College Station, TX 77843-3258, USA.

*Author for correspondence (hqin@.bio.tamu.edu)

H.Q., 0000-0002-0045-5780

Received 7 November 2016; Accepted 11 January 2017

Journal of Cell Science

Journal of Cell Science (2017) 130, 879-891 doi:10.1242/jcs.199117

In most ciliated organisms, the heterotrimeric kinesin-2 motor drives the anterograde transport of IFT particles carrying cargo proteins to the flagellar tip, and the cytoplasmic dynein-1b returns particles carrying turnover products to the base (Cole et al., 1998; Pazour et al., 1999, 1998; Porter et al., 1999; Rosenbaum and Witman, 2002). Since the IFT particle relies on the proper association of multi-subunits, the loss of any one of the IFT particle proteins could have a disastrous effect on the structure of the IFT particle, leading to defects in ciliary assembly and function. Obviously, the subunits in the interface between IFT-B1 and IFT-B2, IFT52, IFT88, DYF-3 and IFT57, are likely to be critical for the integrity of the IFT-B complex. On the other hand, several IFT particle proteins have been shown to directly bind to specific flagellar precursors. For example, IFT46 directly interacts with ODA16 (also known as DAW1), which facilitates the outer arm dynein transport (Hou et al., 2007; Gao et al., 2010; Ahmed et al., 2008). By dimerization, IFT74 and IFT81 cooperatively transport tubulin for cilia assembly (Kubo et al., 2016; Bhogaraju et al., 2013a). IFT56 appears to transport a set of proteins involved in motility (Ishikawa et al., 2014). Consistent with being an IFT particle protein, IFT57 has been shown to be essential for ciliogenesis in several model organisms, including *Caenorhabditis elegans* (Haycraft et al., 2003; Perkins et al., 1986), zebrafish (Cao et al., 2010) and mice (Houde et al., 2006). However, the exact role of IFT57 in the IFT-B complex assembly and cargo transportation is unknown.

In this study, we isolated a mutant containing a hypomorphic allele of *IFT57* in *Chlamydomonas* and analyzed the specific contributions of IFT57 to flagellar assembly and function. The mutant expresses a significantly reduced amount of IFT57. Concomitantly, the amounts of some other IFT-B core proteins also decrease dramatically. Surprisingly, although IFT57 lies at the interface between IFT-B1 and IFT-B2 (Katoh et al., 2016; Taschner et al., 2016), the depletion of IFT57 affects neither the assembly of IFT-B nor the flagellar entry of IFT particles. We also show that, even though a percentage of the *ift57* mutant cells assemble flagella, these flagella have motility defects and display abnormal waveforms. Analysis of the mutant flagellar protein composition shows certain axonemal proteins are drastically changed, suggesting that IFT57 is involved in transporting a specific set of motility-related cargoes.

RESULTS

The *ift57-1* mutant expresses a trace amount of IFT57 due to an insertion in the 5′UTR of the *IFT57* gene

We generated *Chlamydomonas* mutants by random insertional mutagenesis and first screened for phototaxis-defective mutants. Flagellar assembly mutants were found by microscopic observation (Yanagisawa et al., 2014). We further screened a set of mutants with severe flagellar assembly defects by immunoblotting whole-cell extracts with a strong IFT-B antibody anti-IFT46 (Hou et al., 2007). One strain *2P40* was found expressing a highly reduced level of IFT46 and contained a complete hygromycin-resistant gene cassette in the 5′UTR of the *IFT57* loci (Fig. 1A). We renamed the mutant *2P40* as *ift57-1* after backcrossing three times. Since the coding sequence of *IFT57* remained intact, we next evaluated the effect of the insertion by measuring the protein and mRNA abundance of *IFT57* in *ift57-1* cells. The mutant cells expressed ∼5% of wild-type amount of IFT57 at both the protein (Fig. 1B,C) and mRNA level (Fig. 1D). Therefore, the insertion at the 5′UTR did not completely abolish the expression of *IFT57*, but rather reduced its transcriptional efficiency or the stability of its transcripts. Transforming a 7.2-kb genomic fragment containing the *IFT57* gene into the *ift57-1* genome, led to a recovery of *IFT57* expression at both the protein and mRNA level (Fig. 1B–D). Moreover, accompanying the expression of *IFT57*, the flagellar defects associated with *ift57-1* were also rescued (Fig. 2B,C).

Depletion of IFT57 reduces the stability of IFT-B1

The effects of the IFT-B2 protein IFT57 depletion on other IFT particle proteins were examined by immunoblotting assays. Previously characterized IFT-B1 mutants, *ift52*, *ift46* and *ift88*, were included for comparison. Similar to IFT-B1 mutants, *ift57-1* had a normal to slightly elevated cellular level of the IFT complex A protein IFT122 but substantially reduced levels of complex B1 proteins, IFT46, IFT74 and IFT81 (Fig. 1E). However, despite the fact that IFT57 and IFT20 are in the same IFT-B2 subcomplex and directly interact biochemically (Katoh et al., 2016; Taschner et al., 2016), the levels of IFT20 were not reduced but rather increased in *ift57-1* cells (Fig. 1E). Since the IFT20 level was not adversely affected by the depletion of the IFT-B complex, the biochemical stability of IFT20 is independent of the presence of either the IFT-B1 or IFT-B2 subcomplexes.

We then measured mRNA levels and turnover rates of IFT proteins in *ift57-1* to determine whether the reduction in the cellular levels of IFT-B1 proteins were caused by transcriptional inhibition or increased protein degradation. The quantitative real-time PCR (qPCR) results showed that the transcriptional levels of *IFT74* (IFT-B1), *IFT88* (IFT-B1) and *IFT140* (IFT-A) in *ift57-1* were comparable to those in wild-type cells (Fig. 1F). Apparently, the depletion of *IFT57* mRNA did not affect the gene transcriptions of IFT particle proteins. Then, we conducted a time-course cycloheximide treatment to measure the degradation rate of IFT46, which is critical for the stability of IFT-B (Richey and Qin, 2012; Hou et al., 2007), in *ift57-1*. Similar to previous results, IFT46 was very stable in wild-type cells (Fig. 1G), showed a slight decrease in stability in the *ift88* mutant and a dramatic decrease in the *ift52* mutant (Richey and Qin, 2012). In the *ift57-1* mutant, IFT46 exhibited a decreased stability, indicating that IFT57 is important for preventing degradation of IFT complex B proteins. Moreover, when *ift57-1* mutant cells reached the stationary growth phase, the IFT-B complex was quickly degraded (Fig. S1). These results are in agreement with IFT57 as an integral component of the IFT-B complex, and IFT57 depletion results in the destabilized IFT-B complex (Fig. 1G).

The flagellar assembly is compromised when IFT57 is depleted

As the depletion of IFT57 caused a reduction of IFT particles, we asked how the flagellar assembly is affected in *ift57-1* mutant cells. Unlike wild-type *cc125* cells, which contained individual cells with two long flagella (mean±s.d., length=10.55±1.11 µm) (Fig. 2A–C), ∼80% of *ift57-1* total cell population were clusters of four or eight cells encased in mother cell walls (Fig. 2A,B). Close microscopic analyses revealed that at least some cells trapped inside the mother cell walls assembled short flagella (Fig. 2A). The release of daughter cells from mother cell walls depends on a proteolytic enzyme secreted by the flagella of the daughter cells (Kubo et al., 2009). Apparently, *ift57-1* flagella were incapable of secreting a sufficient amount of the enzyme to digest mother cell walls. Moreover, most of the small percentage of liberated individual cells in the *ift57-1* culture were bald, and only a few cells had assembled flagella (2.3%). Occasionally, a cell with near full-length flagella could be observed (Fig. 2A–C). Obviously, the flagellar assembly of *ift57-1* was greatly compromised. These results are consistent with IFT57 being critical for ciliogenesis in other ciliated organisms

Journal of Cell Science (2017) 130, 879-891 doi:10.1242/jcs.199117

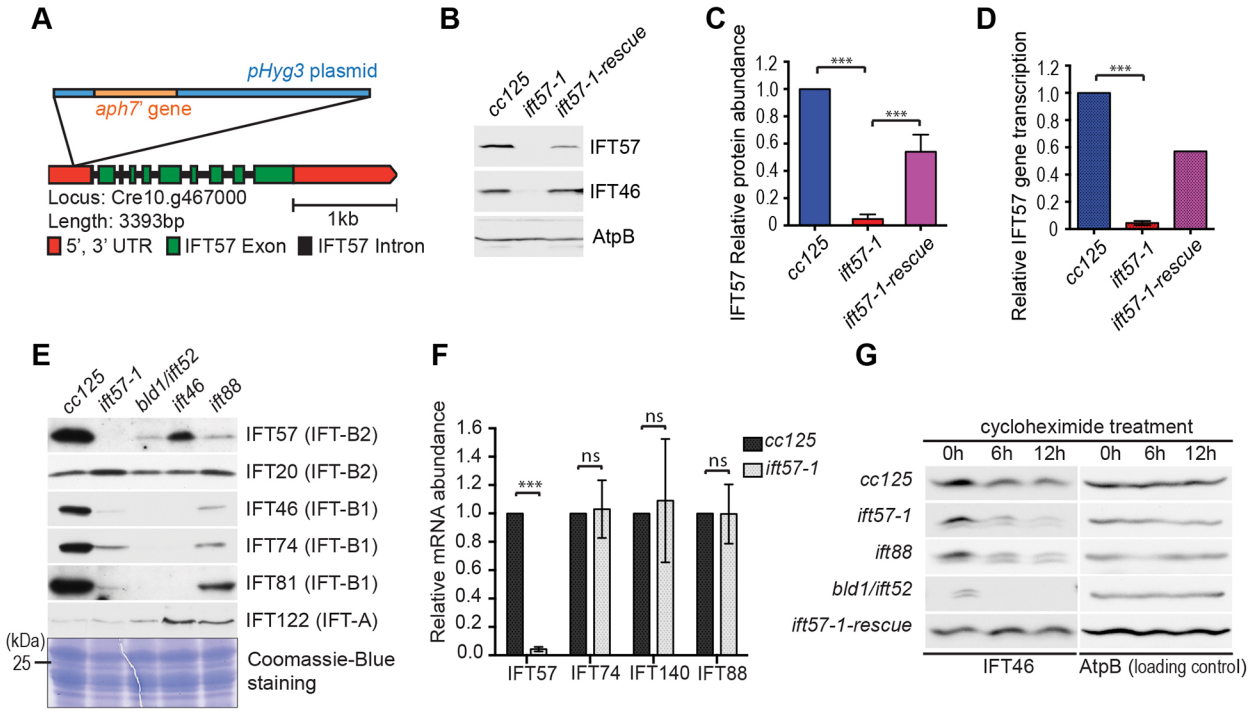

Fig. 1. Characterization of the *ift57-1* mutant. (A) A hygromycin-resistant gene *aph7′* was inserted into the 5′UTR after nucleotide 91 of the *IFT57* gene. (B) The *IFT57* expression at the protein level was reduced in the *ift57-1* mutant. Whole-cell lysates from the wild-type *cc125* and the mutant *ift57-1* cells were probed with antibodies against IFT57 and IFT46. The β-subunit of ATP synthase (AtpB) was used to show equal loadings. (C,D) The *ift57-1* mutant cells had ∼5% of wild-type amount of *IFT57* at the protein (C) and mRNA level (D). IFT57 was recovered to ∼50% of wild-type level in the *ift57-1-rescue* strain. The relative IFT57 abundances were plotted based on the intensity of the bands on immunoblots. The mRNA of *IFT57* was measured by qPCR. Data were collected from three independent experiments. (E) The levels of the IFT-B proteins were severely reduced in *ift57-1*. Whole-cell lysates from *cc125* cells, *ift57-1* cells and cells mutant for three known IFT-B mutants (*bld1*/*ift52*, *ift46* and *ift88*) were probed with antibodies against IFT complex proteins. (F) IFT genes (*IFT74*, *IFT140* and *IFT88*) were expressed at similar levels in *cc125* and *ift57-1* cells. The graph was generated from three independent qPCR results. (G) The stability of IFT46 was reduced in *ift57-1* cells. A 12-h time-course treatment with cycloheximide was used to examine degradation rates of existing proteins. Whole-cell extracts were probed with anti-IFT46 antibody. AtpB was used to ensure equal loadings. In all panels, the error bars represent s.d. ***P<0.001; ns, not significant.

(Perkins et al., 1986; Haycraft et al., 2003; Houde et al., 2006; Cao et al., 2010).

Autotrophic condition promotes flagellar assembly and IFT particle protein expression

There are two common media for *Chlamydomonas* culture, TAP and M1. The main difference between them is the TAP provides carbon nutrients, while the M1 does not. Consequently, the cell growth in M1 medium is entirely dependent on photosynthesis. *Chlamydomonas* cells grow much faster in TAP medium. However, the cells, especially the flagellar-defective mutants, flagellate much better when cultured in M1 medium. Therefore, M1 medium is often used to encourage flagellar assembly. When *ift57-1* cells were grown in M1 medium, cell clumps seen in TAP medium largely disappeared (Fig. 3A). Moreover, ∼75% of cells assembled relative long flagella (≥6 µm). Obviously, when the *ift57-1* cells were cultured autotrophically in M1 medium the flagellar assembly was much less adversely affected.

Immunoblotting results showed that both the wild-type and the *ift57-1* mutant cells clearly expressed a higher amount of IFT particle proteins when the cells were cultured in M1 compared to in TAP medium (Fig. 3B). Therefore, the autotrophic culture condition increased the cellular concentrations of IFT particle proteins in general, which led to the improved flagellar assembly of *ift57-1* cells cultured in M1 medium.

We then asked whether *ift57-1* cells with long flagella contain more IFT particles than those with short or no flagella. Because only the cells bearing long flagella swam effectively towards light while the ones with short or no flagella could not (Fig. 3C,D), we were able to separate the two types of cells by photoaccumulation. Immunoblotting analysis revealed that cells with longer flagella indeed had a higher *IFT57* expression, while the ones with shorter or no flagella had a much lower amount of IFT57 (Fig. 3E). Taken together, these results clearly demonstrate that in *ift57-1* cells the *IFT57* expression positively correlates with the status of flagellar assembly.

IFT particle proteins localize to the basal body in *ift57-1* mutant cells

To examine whether the IFT-B complex still localized to the basal body in *ift57-1* cells, we checked the cellular distribution of a few IFT proteins by indirect immunofluorescence staining (Fig. 4). The anterograde motor subunit FLA10 was used as a basal body marker (Deane et al., 2001; Cole et al., 1998; Richey and Qin, 2012). We chose the cells cultured in TAP medium and that had tiny or no flagella for staining. These cells presumably had very little *IFT57* expression (Fig. 1B,C). Results showed that in both wild-type and the *ift57-1* mutant cells, the IFT-A protein IFT139 colocalized with FLA10 at the basal body. Thus, the IFT-A complex was not affected by the depletion of IFT57. In contrast, changes were noticed for IFT-B proteins. In *cc125* cells, all three IFT-B proteins colocalized with IFT122 (IFT-A) and FLA10. In the mutant *ift57-1*, IFT46 (IFT-B1) was clearly localized to the basal body. IFT81 (IFT-B1) and IFT172 (IFT-B2) were also consistently found at the basal body.

Journal of Cell Science (2017) 130, 879-891 doi:10.1242/jcs.199117

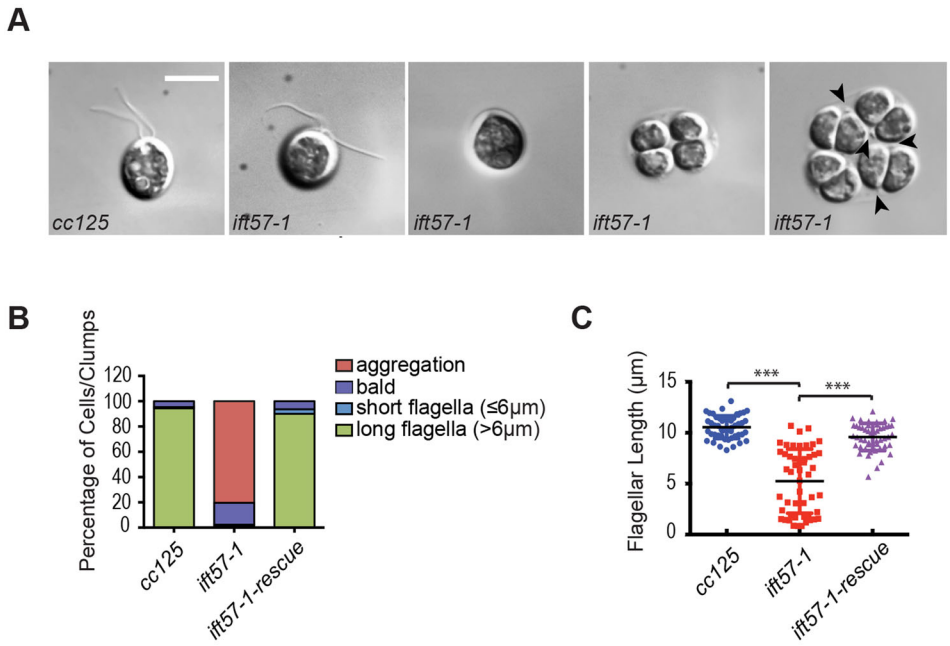

Fig. 2. IFT57 depletion causes flagellar assembly defects. (A) *Ift57-1* mutant cells displayed a range of flagellar assembly defects. The control wild-type *cc125* cells were rarely seen in clusters, and over 90% of cells had full-length flagella. When *ift57-1* were cultured in TAP medium, most cells were seen in clumps. Hatched individual cells assembled no or short flagella. Tiny flagella were occasionally seen on cells trapped inside mother cell walls (highlighted by black arrowheads). Scale bar: 10 µm. (B) 300 randomly picked cells or cell clumps from each strain were analyzed. The graph shows the percentage of cells or cell clumps that: (1) assembled long flagella (>6 µm); (2) assembled short-length flagella (≤6 µm); (3) were bald; or (4) were in aggregates. One representative result is shown here. Similar results were observed in multiple repeats. (C) 50 flagellated cells from each culture were randomly selected for length measurement. The mean±s.d. flagellar length of *ift57-1* mutant cells (5.25±3.15 µm) was shorter than that of wild-type cells (10.55±1.11 µm). The defect was partially recovered in the rescue strain *ift57-1-rescue* (9.58±1.34 µm).

However, the labeling of IFT81 (IFT-B1) was more dispersed, similar to the background dots in wild-type cells. In contrast, although only a small proportion of IFT172 reached the basal body, most IFT172 did not disperse throughout the cell but rather accumulated just beneath the basal body. This cellular distribution pattern of IFT172 was also observed in other IFT-B mutants (Fig. S2). Overall, the localization of IFT particle proteins as well as the IFT motor FLA10 appeared to be normal.

CrDYF-3 is an IFT particle protein of *Chlamydomonas* and co-purifies with IFT57

IFT57, together with *Chlamydomonas* DYF-3 (denoted CrDYF-3), plays a crucial role in IFT-B1 and IFT-B2 connection through contacts with IFT52–IFT88 (Taschner et al., 2016; Katoh et al., 2016). To understand the relationship between these two subunits, polyclonal anti-CrDYF-3 antisera was employed to detect the endogenous CrDYF-3 on western blots. The antibody recognized a single band, which is slightly smaller than IFT57 of flagellar extracts (Fig. 5A).

The flagellar entry of IFT particles solely depends on the anterograde motor kinesin-II (Kozminski et al., 1995). The mutant *fla10-1* harbors a point mutation in the kinesin-II motor subunit FLA10, and is functionally normal in flagellar assembly at the permissive temperature (18°C) but has no anterograde IFT at the non-permissive temperature (32°C) (Walther et al., 1994; Cole et al., 1998). Similar to IFT particle subunits IFT139 and IFT74, the amount of CrDYF-3 was significantly decreased in the flagella of the *fla10-1* mutant at 32°C (Fig. 5B). This result revealed that, like other IFT proteins, the entrance of CrDYF-3 into flagella is FLA10 dependent.

We then utilized sucrose density gradient centrifugation to determine the sedimentation pattern of CrDYF-3 (Fig. 5C,D). On the gradient, CrDYF-3 co-eluted with IFT57 in the 16S fractions. The corresponding band from the Coomassie-Blue-stained gel (Fig. 5D) was analyzed by mass spectrometry. Only two proteins, IFT57 and CrDYF-3, were identified from the band (data not shown), confirming the identity of CrDYF-3. Moreover, we noticed that IFT-B1 and IFT-B2, the two subcomplexes of IFT-B, did not completely co-sediment on the gradients (Fig. 5C). IFT-B1 subcomplex proteins IFT81 and IFT70 co-eluted in fractions 8 and 9, while IFT-B2 subunits IFT57 and CrDYF-3 were concentrated in fractions 9 and 10. Therefore, IFT-B1 and IFT-B2 were biochemically separated on the gradients. These results suggest that the association and disassociation between IFT-B1 and IFT-B2 could be subjected to regulation *in vivo*.

The purification of recombinant CrDYF-3 protein alone is difficult since the protein appears to be structurally unstable and is prone to form aggregates. DYF-3 becomes soluble only when it co-expressed with IFT57 (Taschner et al., 2016). Indeed, a few attempts to purify the soluble CrDYF-3 protein alone from *E. coli* were unsuccessful. However, when we mixed two crude *E. coli* extracts that contained the expressed tagged CrDYF-3 and IFT57 proteins, respectively, we were able to co-purify CrDYF-3 and IFT57 (Fig. 5E). This result supports the hypothesis that CrDYF-3 and IFT57 directly interact.

IFT57 depletion does not affect the flagellar entry of IFT particles and the assembly of IFT-B complex

To address how the depletion of IFT57 affects the distribution of IFT particles to flagella, we checked the levels of IFT57 as well as

Journal of Cell Science (2017) 130, 879-891 doi:10.1242/jcs.199117

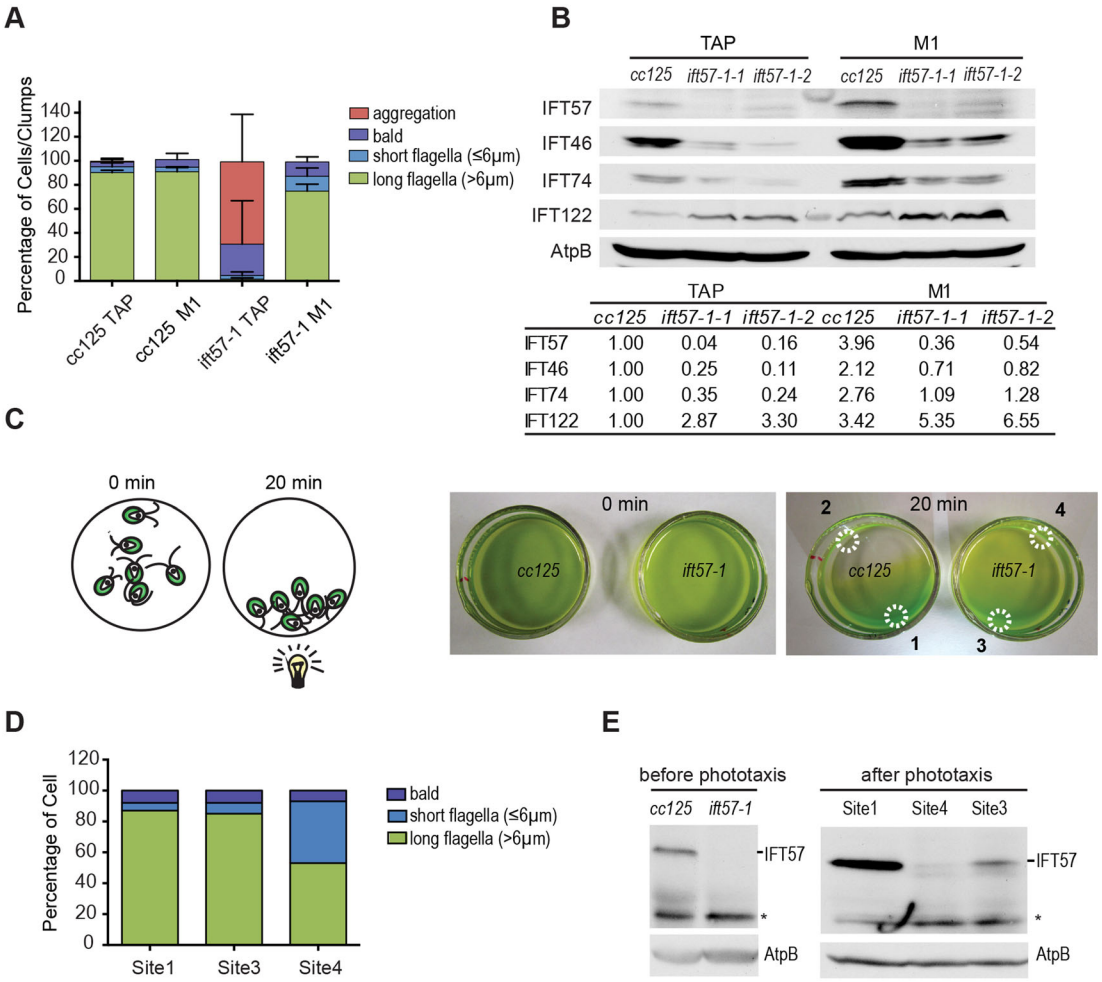

Fig. 3. Autotrophic condition promotes flagellar assembly in *ift57-1* cells. (A) The flagella were less abnormal in *ift57-1* mutant cells grown in M1 than in cells grown in TAP medium. Data were collected from three independent experiments (total *n*=300, individual cells plus cell clumps per experiment). Error bars represent s.d. (B) Immunoblots of whole-cell lysates from cells cultured in TAP or M1 medium probed with antibodies against IFT particle proteins as indicated. Lanes between the 'TAP' and 'M1' samples are molecular mass markers. The samples '*ift57-1*-1' and '*ift57-1*-2' are two independent samples of whole-cell extracts of *ift57-1* cells. The table shows the relative protein abundances based on the intensity of the bands on immunoblots. The values for the bands in the lane 'cc125 TAP' were set as 1.00. AtpB bands were used to normalize the variations caused by loadings. (C) By using the photoaccumulation assay, the wild-type *cc125* or the mutant *ift57-1* cells were separated into two groups; one that swam to light (1 and 3), and the other group that failed to swim towards the light source (2 and 4). (D) Cells taken from sites 1, 3 and 4 (*n*=300) were observed under the microscope. The graph shows the percentage of cells that were bald, had short flagella or had long flagella. Site 2 was devoid of cells because of strong phototaxis effects. The result from one experiment is shown here. Similar results were obtained from three repeats. (E) Immunoblots of whole-cell lysates showed cells from site 3 expressed a higher level of IFT57 than those from site 4. Antibody against AtpB was used to ensure equal loadings. Similar results were observed in three repeats. *, nonspecific bands on anti-IFT57 immunoblots.

several subunits of IFT-A and IFT-B in isolated *ift57-1* flagella (Fig. 6A,B). *Ift57-1* flagella showed a reduced level of IFT57 compared to wild-type. Two complexes, the IFT-A and BBSome (an IFT cargo complex that carries specific cargoes in and out of cilia), remained at wild-type levels. Strikingly, the flagellar content of IFT-B2 proteins CrDYF-3 and IFT172 as well as that of the IFT-B1 subunits IFT46, IFT56 and IFT81 was not reduced. This result revealed that, in *ift57-1* mutant flagella, IFT57 was at a sub-stoichiometric level relative to the rest of the IFT-B proteins (Fig. 6A,B). The IFT-B complex assembly appeared to be normal in *ift57-1* cells (Fig. 6C). We also examined the movement of IFT trains in *ift57-1* mutant flagella with total internal reflection fluorescence (TIRF) microscopy followed by kymograph analysis (Engel et al., 2009a,b; Lechtreck et al., 2009). A fusion between GFP and the non-motor subunit of the IFT anterograde motor FLA10-kinesin-II, denoted KAP–GFP, underwent a prominent anterograde IFT with similar speeds to that seen in wild-type (Fig. 6D,E; Movies 8 and 9), indicating that the IFT movement is likely unaffected in *ift57-1* flagella. Therefore, despite the fact that IFT57 sits at the interface between the IFT-B1 and IFT-B2 complexes (Katoh et al., 2016; Taschner et al., 2016), these results collectively show that IFT57 is not essential for the assembly of IFT-B nor is it required for the flagellar entry of IFT particles. Because CrDYF-3 presented at the wild-type level in *ift57-1* mutant flagella, we postulated that CrDYF-3, the other interface subunit of IFT-B2, is sufficient to mediate the binding between IFT-B1 and IFT-B2.

IFT57 is required for establishing normal flagellar waveforms

While performing the photoaccumulation experiments, we noticed that within the population of *ift57-1* cells that failed to swim towards the light source, ∼50% percent of cells assembled flagella longer than 6 μm (Fig. 3D). We thought that their failure to swim towards the light may be due to motility defects. We checked the swimming

Journal of Cell Science (2017) 130, 879-891 doi:10.1242/jcs.199117

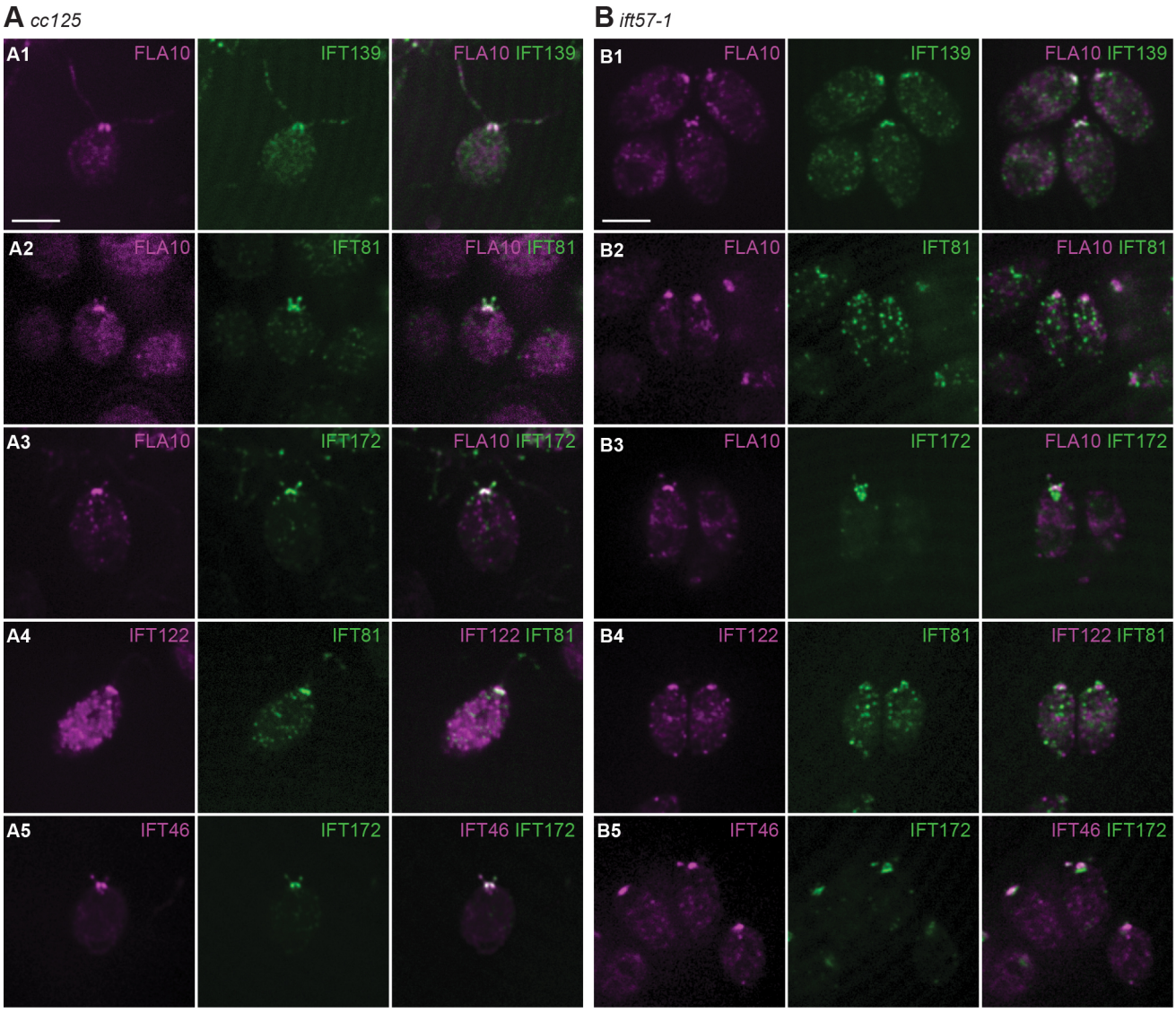

Fig. 4. Effects of IFT57 reduction on cellular localization of IFT-B proteins. Immunofluorescent stainings of the wild-type *cc125* (A) and the mutant *ift57*-1 (B) cells. Antibodies against IFT proteins, IFT139 (A), IFT122 (A), IFT172 (B), IFT81 (B), IFT46 (B), and FLA10, were used in the stainings. All analyzed cells showed consistent localization patterns as depicted in A1, B1, A2, B2, A4 and B4. The IFT172 accumulation beneath the basal body (depicted as in B3 and B5) was often detected in *ift57-1* mutant cells (49 out of 61), while it was rarely seen in *cc125* (2 out of 25). Scale bars: 10 µm.

patterns of wild-type and *ift57-1* cells. Most wild-type cells swam in a relatively continuous smooth path (Fig. 7A1; Movie 1). However, the trajectories of *ift57-1* cells revealed that they either frequently stopped or exhibited a spiral pattern, leading to a decreased forward motion (Fig. 7A2–A4; Movies 2 and 3). These movements were not seen in wild-type cells. In different batches of *ift57-1* cells, the severity of swimming defects was variable (Fig. 7A). The swimming paths of wild-type cells were always consistent, indicating that their flagella were well equipped to tolerate fluctuating environmental changes.

To closely watch flagellar waveforms, we recorded single-cell movements in wild-type and *ift57-1* cells. Consistent with previous reports, wild-type cells swam forward using an asymmetrical flagellar waveform (Fig. 7B1; Movie 4). One beating cycle of wild-type flagella consisted of a recovery stroke (Fig. 7B1, frames 1–6) followed by a power stroke (Fig. 7B1, frames 7–12). However, the waveform was abnormal, and the beatings of the two flagella of *ift57-1* cells were uncoordinated (Fig. 7B2,B3; Movies 5–7). The abnormal waveform caused the cells to restlessly tumble at the same spot, move around in circles or take spiral paths (Fig. 7A). In the *ift57-1-rescue* strain, both the swimming path and the flagellar waveform were normal (data not shown).

The level of the inner dynein arm I1 subunit IC97 is greatly reduced in *ift57-1* mutant flagella

We checked levels of several motility-related axonemal proteins in whole flagellar samples by immunoblotting. While the levels of the inner dynein arm I1 subunits IC138 (Bower et al., 2009) and IC140 (Perrone et al., 1998; Yang and Sale, 1998), microtubule doublet inner junction protein FAP20 (Yanagisawa et al., 2014), outer dynein arm components LC1 and IC69 (King, 2012), radial spoke protein RSP3 (Yang et al., 2006), and axonemal protein MBO2 (Tam and Lefebvre, 2002) were near wild-type levels, the amount of IC97 (Wirschell et al., 2009) was significantly reduced in the *ift57-1* mutant flagella (Fig. 8). The IC97 expression in the *ift57-1* mutant at the whole-cell level was normal (data not shown). Thus, the

Journal of Cell Science (2017) 130, 879-891 doi:10.1242/jcs.199117

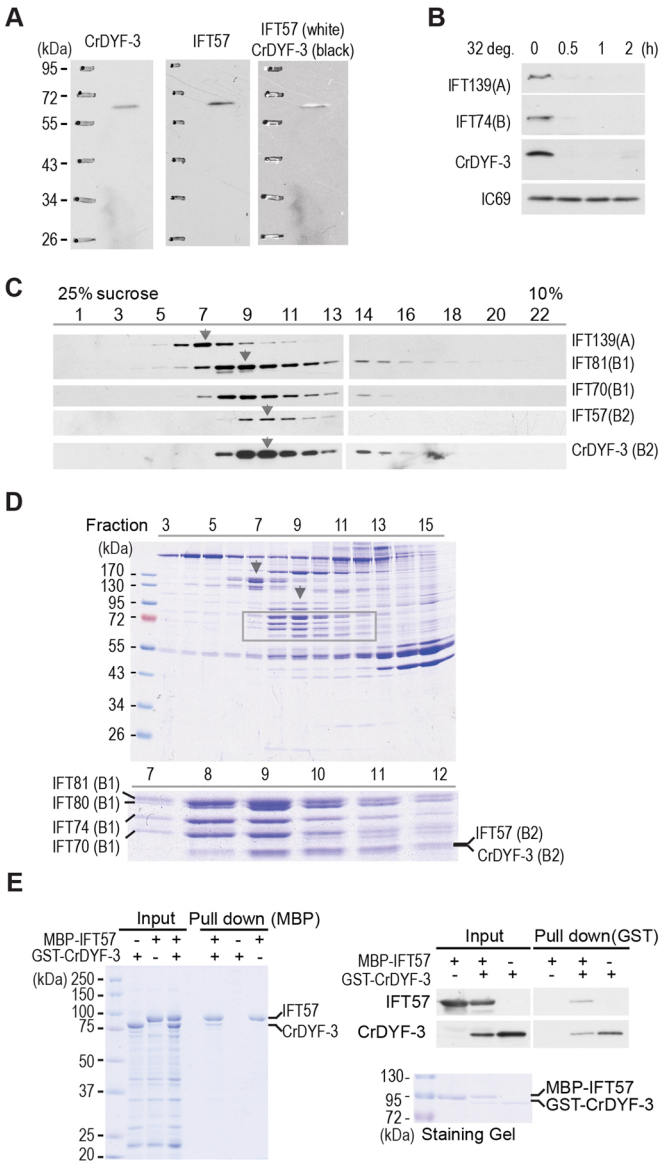

Fig. 5. CrDYF-3 is an IFT-B2 protein in *Chlamydomonas*. (A) The size of CrDYF-3 was slightly smaller than that of IFT57 based on two immunoblots of a single membrane. The membrane was first probed with anti-CrDYF-3 (a rabbit antibody), and then with anti-IFT57 (a mouse monoclonal antibody). (B) Immunoblots of flagellar extracts showed that CrDYF-3 disappeared along with IFT139 and IFT74 from *fla10-1* flagella at 32°C. Axonemal protein IC69 was used as an equal loading control. (C) CrDYF-3 co-eluted with IFT57 on sucrose density gradients. Immunoblots of gradient fractions show the sedimentation peaks of the IFT-A protein IFT139, and IFT-B proteins IFT81, IFT70, IFT57 and CrDYF-3. Arrowheads highlight the peak fractions of each labeled protein. (D) The upper panel is a Coomassie-Blue-stained gel of gradient fractions showing protein bands for IFT particle proteins. Gray arrowheads highlight the fractions containing IFT-A and IFT-B, respectively. The lower panel shows the positions of IFT57 and CrDYF-3 along with a few other IFT-B proteins. (E) CrDYF-3 interacts with IFT57. MBP-tagged IFT57 and GST-tagged CrDYF-3 were expressed in *E.coli* and used for *in vitro* binding assay. The left panel (Coomassie-Blue-stained gel) shows that immobilized MBP–IFT57 pulled down CrDYF-3 protein. Immunoblots probed with antibodies against IFT57 and CrDYF-3 on the right panel show that immobilized GST–CrDYF-3 retained IFT57 protein. The Coomassie-Blue-stained gel at the bottom was used to show the proteins used in the input for the pulldown analysis.

reduction in the level of IC97 in *ift57-1* flagella was not due to inhibition of expression but caused by a low efficiency in flagellar entry, retention on the axoneme or both.

To further access the effect of depletion of IFT57 on flagellar composition, we separated the flagellar proteins of *cc125* and *ift57-1* cells by electrophoresis (Fig. S3). On Coomassie-Blue-stained gels, one specific band at ∼25 kDa consistently appeared in the *ift57-1* sample. In contrast, it was completely invisible or was just faintly visible in the wild-type sample. Furthermore, a few additional proteins showed altered amounts. The identities of these proteins are still unknown.

DISCUSSION

Here, we report how IFT57 functions in flagellar assembly and motility in *Chlamydomonas*. The hypomorphic mutant *ift57-1* expressed a greatly reduced amount of IFT57 and was poorly flagellated (Figs 1 and 2). At the whole-cell level, the levels of IFT57 along with other IFT-B proteins were highly reduced, indicating that IFT57 is important to maintain the stability of the IFT-B complex (Fig. 1). Strikingly, although the flagellar level of IFT57 was reduced, the levels of other IFT proteins were not concomitantly affected by the depletion of IFT57 (Fig. 6). In *ift57-1* flagella, the levels of all tested IFT particle proteins, except IFT57, were not reduced. Additionally, the anterograde IFT motility in flagellated *ift57-1* cells was also comparable to that in wild-type cells (Fig. 6D,E). Therefore, although IFT57 is important for flagellation because it acts to maintain the cellular amount of IFT particles, it is not essential for the IFT complex assembly or for the flagellar entry of IFT particles. Another noted defect in *ift57-1* cells is that they have defective flagellar waveforms and/or beating coordination (Fig. 7). Several flagellar proteins, including the intermediate chain of I1 dynein IC97 were drastically altered in *ift57-1* flagella (Fig. 8; Fig. S3), suggesting that IFT57 is involved in the transport of a specific set of motility-related cargoes.

Here, we show that the IFT57-depleted *Chlamydomonas* cells had severely reduced and unstable IFT-B1 proteins (Fig. 1E,G). Therefore, although being an IFT-B2 subunit, IFT57 is very important for the stability of IFT-B1. A previous report shows that IFT57 works as a linkage between IFT172 and IFT20 in IFT-B2 (Katoh et al., 2016). Interestingly, our work finds that the depletion of IFT57 does not affect the expression of IFT172 and IFT20 (Fig. 1E; Fig. S2). These two proteins are likely biochemically stable.

In this study, two lines of evidence demonstrate that IFT57 is not essential for the assembly of the IFT-B complex. Firstly, the IFT-B complex from *ift57-1* whole-cell extracts still sedimented at about 16S, demonstrating that IFT-B is relatively intact (Fig. 6C). Secondly, the low cellular pool of IFT-B proteins did not lead to a low flagellar level of IFT-B proteins. Instead, although the level of IFT57 was significantly reduced, all other IFT-B proteins were at wild-type levels or an even higher level in *ift57-1* flagella (Fig. 6A,B). Moreover, the IFT-B complex assembled in *ift57-1* mutant flagella was apparently functional since it underwent IFT movement at the wild-type velocity (Fig. 6D,E). These results strongly support that the IFT-B complex assembles and functions normally in the absence of IFT57. Taken together, we conclude that IFT57 is important for maintaining the stability of IFT-B, but is likely dispensable for the IFT-B complex formation and IFT motility.

The recent work from both the Lorentzen and the Nakayama laboratories concludes that IFT57 and/or DYF-3 (IFT-B2), and IFT52 and IFT88 (IFT-B1) are essential for linking IFT-B1 and IFT-B2 together (Taschner et al., 2016; Katoh et al., 2016). However, they disagree on how IFT57 functions. By using purified *E. coli*-expressed purified *Chlamydomonas* proteins, Lorentzen and colleagues show that IFT57 and DYF-3 directly interact to form a

Journal of Cell Science (2017) 130, 879-891 doi:10.1242/jcs.199117

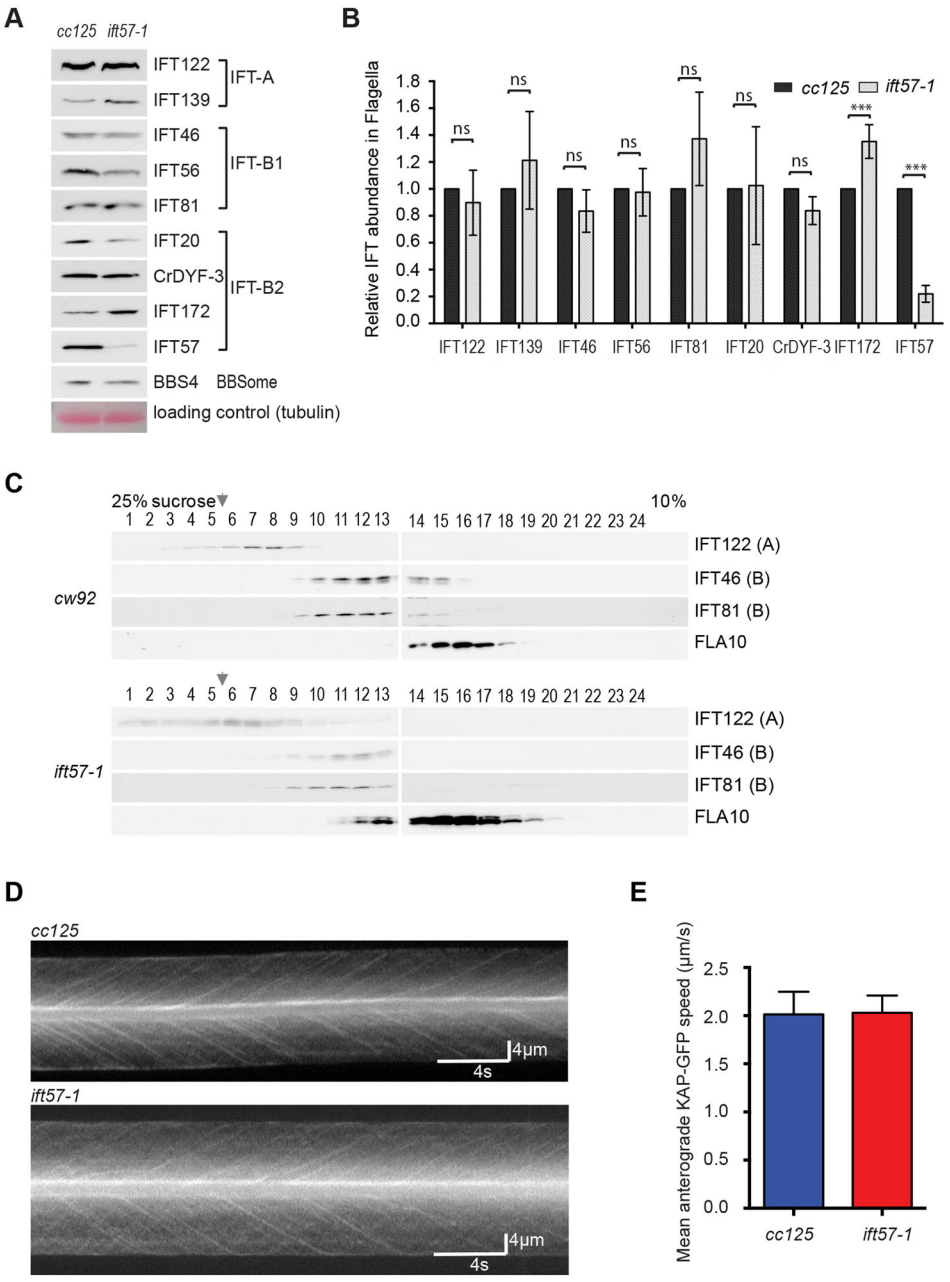

Fig. 6. IFT57 is not essential for IFT complex B assembly, its entry to flagella or its motility inside flagella. (A) Immunoblots of isolated flagella from *cc125* and *ift57-1* cells showed that although the level of IFT57 was dramatically reduced in *ift57-1* flagella, the levels of other IFT proteins and BBS4, one subunit of BBSome, were comparable to those in *cc125* cells. Ponceau-stained tubulin was used as the equal loading control. (B) Quantitative analysis of IFT protein levels in *cc125* and *ift57-1*. The graph was generated from four independent experiments. (C) Immunoblots showed that the sedimentation peaks of both IFT-A (IFT122) and IFT-B (IFT46 and IFT81) proteins were the same on sucrose density gradients from the control *cw92* and the mutant *ift57-1* whole-cell extracts. FLA10 (at 10S) and Rubisco (at 19S) were used as references to ensure the gradients were prepared identically. Peaks of Rubisco (at 19S) are indicated with arrowheads. (D) Kymographs revealed the motility of KAP–GFP in flagella of *cc125* and *ift57-1* cells. (E) The mean speed of KAP-GFP showed the anterograde IFT movement in *ift57-1* was normal. In all panels, the error bars represent s.d.

dimer, which is essential for binding to IFT52 or IFT88 (Taschner et al., 2016). However, they cannot tell which one of the two proteins, or both, is sufficient for binding to IFT52 or IFT88 since it is technically difficult to purify individual proteins. On the other hand, using overexpressed human or mouse IFT proteins in mammalian culture cells the Nakayama group shows that IFT57 and DYF-3 do not interact directly. They rely on IFT20 to bridge them together (Katoh et al., 2016). In this study, we have confirmed that recombinant *E. coli*-expressed *Chlamydomonas* IFT57 and CrDYF-3 can be co-purified, supporting the idea that these two proteins form a dimer (Fig. 5D,E). Moreover, we have shown that, in *ift57-1* mutant flagella, the levels of IFT57 were significantly reduced, while those of CrDYF-3 and other IFT-B proteins remained at the wild-type level (Fig. 6A,B). Clearly, in *ift57-1* mutant flagella IFT57 was at a much lower level relative to CrDYF-3. Because CrDYF-3 presented at a molar ratio relative to other IFT-B proteins when IFT57 was depleted (Fig. 6A,B), we propose that CrDYF-3 alone is sufficient to mediate the integration of IFT-B1 and IFT-B2. On the other hand, CrDYF-3 and IFT57 have similar predicted 3D structures (Taschner et al., 2016). It is possible that although both CrDYF-3 and IFT57 sit at the interface between IFT-B1 and IFT-B2, either one of them is sufficient to bridge IFT-B1 and IFT-B2 together. The binding of IFT57 onto the complex might also stabilize the structure of IFT-B since the IFT57-deficient-IFT-B complex was unstable, and prone to degradation in the cell body (Fig. 1G). This notion is supported by the fact that when the IFT57-deficient IFT-B complex enters flagella, it could accumulate inside the flagellar compartment (Fig. 6A,B) since the flagellum contains few proteases (Pazour et al., 2005).

In this study, we noticed that the flagellated *ift57-1* cells, even the ones with relatively long flagella, showed certain degrees of motility defects (Figs 3C,D and 7A). Further flagellar waveform analysis revealed that in *ift57-1* mutant cells, the beatings of the two flagella were uncoordinated (Fig. 7B). IFT57 and IFT20 have been

Journal of Cell Science (2017) 130, 879-891 doi:10.1242/jcs.199117

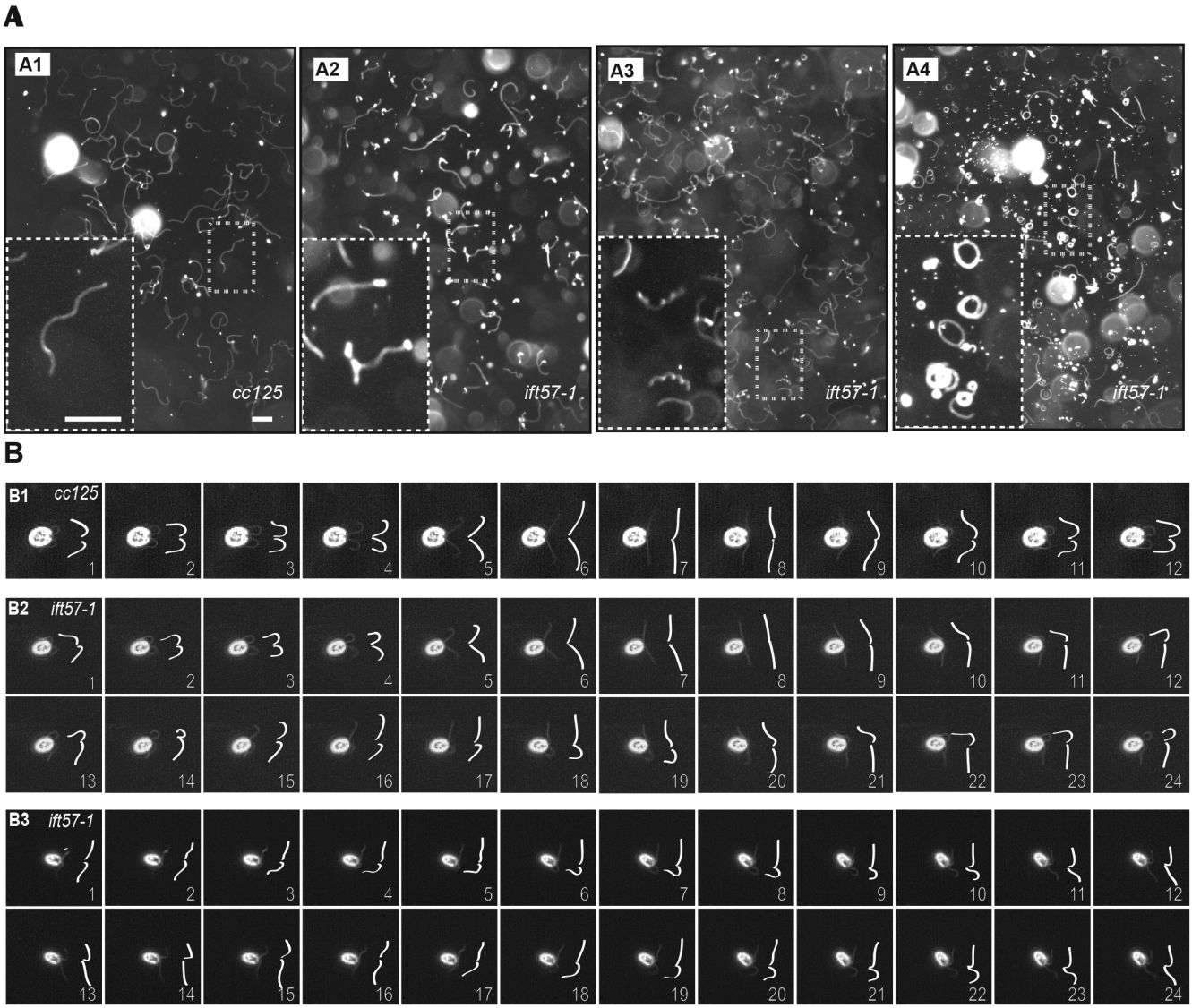

Fig. 7. IFT57 is essential for normal flagellar motility. (A) Cell swimming paths were recorded by imaging cells with 2 s exposures in the dark-field view. A2, A3 and A4 are representative recordings of swimming paths of *ift57-1* from three batches of cells; A1 shows a *cc125* cell. Enlarged dotted regions are for detailed viewing of individual swimming paths. Scale bars: 100 µm. (B) One beating cycle of wild-type cell flagella consists of a recovery stroke (B1 frames 1–6) followed by a power stroke (B1 frames 7–12). The waveform of *ift57-1* was abnormal (B2) or uncoordinated (B3). These continuous frames were taken from high-speed recordings (600 fps) of *cc125* and *ift57-1* cells under microscopes.

previously proposed to facilitate the dissociation between the anterograde motor kinesin-II and IFT particles when they reach the flagellar tip (Krock and Perkins, 2008). However, upon examining the motility of the anterograde motor subunit KAP–GFP in *ift57-1* mutant flagella (Fig. 6D,E), we observed no retrograde tracks, indicating that kinesin-II dissociates from IFT particles at the correct time normally. Moreover, the anterograde IFT speed was not affected at all. Therefore, the IFT movement is normal in *ift57-1* mutant flagella. However, the IFT57-deficient IFT particles, although they underwent IFT movement, may have a reduced efficiency in transporting specific sets of flagellar motility components. In *ift57-1* flagella, the level of the intermediate chain of I1 dynein IC97 decreased dramatically (Fig. 8). IC97 is a regulatory subunit of I1 and required for I1-dynein-mediated control of microtubule sliding *in vitro* (Wirschell et al., 2009). The low level of IC97 in *ift57-1* flagella is likely responsible for the flagellar waveform defects.

IFT particles deliver different types of structural and functional cargoes in and out of the flagellum. IFT proteins use their cargo-binding sites to transport flagellar precursors for assembly and function (Bhogaraju et al., 2013a,b; Eguether et al., 2014; Ishikawa et al., 2014; Hou et al., 2007; Ahmed et al., 2008; Kubo et al., 2016; Lechtreck, 2015; Wren et al., 2013; Lechtreck et al., 2009; Mukhopadhyay et al., 2010). The I1 dynein complex is pre-assembled in the cytoplasm as a 20S complex including IC140, IC138, IC97 and other subunits, and then delivered to flagella by IFT with assistance of the adaptor IDA3 (Viswanadha et al., 2014). Although IC97 is a subunit of the I1 dynein complex, it is not a structural component of I1, nor is it required for I1 dynein axonemal assembly (Wirschell et al., 2009). It could be that IFT57 directly binds to IC97. Alternatively, the structural change in IFT particles caused by IFT57 depletion might reduce its efficiency in transporting IC97 into flagella. Moreover, a few unknown proteins also changed their levels in the flagella (Fig. S3). These

Journal of Cell Science (2017) 130, 879-891 doi:10.1242/jcs.199117

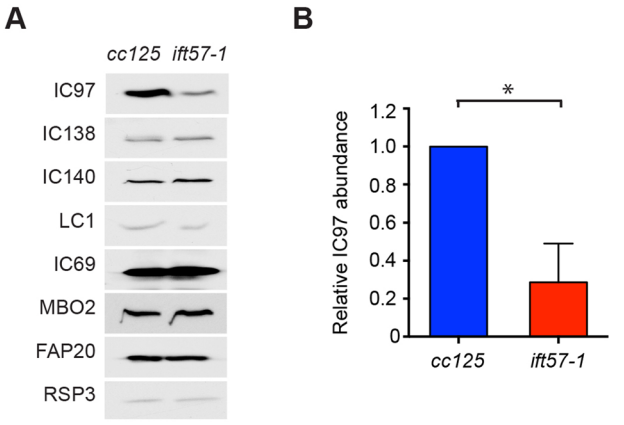

Fig. 8. The level of the axonemal protein IC97 is decreased in *ift57-1* flagella. (A) Immunoblots of isolated flagella were probed with the indicated antibodies. Among all examined axonemal proteins, only the level of IC97 was decreased in *ift57-1* flagella. (B) The relative IC97 protein abundances in the flagellar extracts of *cc125* and *ift57-1*. The graph shows the intensity of the bands on immunoblots from three independent results.

changes may block IC97 binding onto the axoneme, causing it to be depleted from flagella. Future research is needed to address which of the above hypothetic scenarios is correct.

MATERIALS AND METHODS

Strains and culture conditions

The mutant *ift57-1*, the rescue strain *ift57-1-rescue*, and *ift57-1 fla3-1b::KAP-GFP* were made in this study. All other strains were obtained from the *Chlamydomonas* Center (http://chlamycollection.org/). Strains were maintained on Tris-acetate-phosphate (TAP) plates. Cells were cultured in either TAP or M1 liquid medium with constant aeration in a plant growth chamber (Conviron, Manitoba, Canada) at 21°C with continuous light. M1 medium was used to culture cells in experiments for Figs 3C,D,E, 6D,E, and 7A. TAP medium was used for experiments shown in Figs 1, 2, 4, 5B,C,D, 6A,B,C, 7B, 8, Figs S1, S2, and S3. The medium used for experiments shown in Fig. 3A and B are labeled on the figure.

Ift57-1 mutant isolation and mutation mapping

The mutant *2P40* was selected from a set of flagellar assembly mutants containing a hygromycin-resistant *pHyg3* insertion. The insertion site was mapped using a long-and-accurate (LA) PCR *in vitro* cloning kit from Takara (Japan) with modifications. Briefly, enzymes (*Pst*I, *Hin*dIII, *Sac*II, *Nco*I and *Apa*L1) with cutting sequences frequently found in *C. reinhardtii* genome were used to digest genomic DNAs. Digestion products were ligated to short linkers and then used as template for nested PCRs. The primers were based on tagged sequences on both ends of the insertion site. Specifically amplified fragments were then sequenced to identify the insertion site. The *2P40* strain was backcrossed and was called *ift57-1*.

Rescue of *ift57-1*

We used the *Chlamydomonas* bacterial artificial chromosome (BAC) clone 13E3 (http://www.genome.clemson.edu/), which contains the *IFT57* gene, to rescue *ift57-1* cells. The linearized 13E3 was co-transformed with the paromomycin-resistant *pSI103* plasmid for selection. Before transformation, we treated cells with gametic autolysin for 15–20 min to dissociate cell clumps. Transformation was carried out by electroporation as described with modifications (Pollock et al., 2004). Cells were re-suspended in TAP liquid medium containing 60 mM sorbitol, and then transferred to a 4 mm electroporation cuvette. After adding ∼300 ng of linearized *pSI103* and 900 ng of linearized 13E3, cells were chilled on ice for 5 min, and then electroporated in an ECM630 electroporator (BTX, USA) with the following parameters: capacitance, 50 µF; resistance, 650 Ω; and voltage, 825 V. Transformants were obtained from TAP plates containing 10 ng µl^{-1} paromomycin and screened for recovered swimming. Integration of *IFT57* gene was confirmed by PCR using *IFT57* gene-specific primers, *IFT57*-51-69-F and *IFT57*-515-535-R (Table S1). Expressions of *IFT57* were confirmed by western blotting. We chose one of the rescue colonies for detailed analysis, and named it *ift57-1-rescue*.

Comparison of effects of different types of media on flagellar assembly

Ift57-1 and *cc125* cells from fresh TAP plates were transferred to TAP and M1 liquid medium, respectively, and were shook under light at 110 rpm for 3 days. Supernatants without visible cell clumps were then transferred to fresh TAP or M1 medium. After culture for 3 days, 300 randomly picked cells or cell clusters from each flask (TAP *cc125*, TAP *2P40*, M1 *cc125*, and M1 *2P40*) were analyzed. Cells were divided into four categories: (1) aggregate, four or more than four cells formed clumps; (2) bald, single cells with no flagella; (3) short flagella, single cells with flagella shorter than half the length of wild-type flagella (≤6 µm); (4) long flagella, single cells with flagella longer than half the length of wild-type flagella (>6 µm).

Antibodies and immunoblotting assay

The polyclonal rabbit anti-CrDYF-3 antibody was produced by Bethyl Laboratories, Inc (Montgomery, TX). The immunogen is an internal peptide (N-CLYDALGQEPELREHR-C) of the CrDYF-3 protein. The peptide was synthesized, purified by high-performance liquid chromatography (HPLC), and verified by mass spectrometry. The peptide was conjugated to KLH before being used for immunization. The antisera were affinity purified before being used in immunoblotting.

Other antibodies used in this study include antibodies against IFT proteins: FLA10, IFT57, IFT81, IFT139, IFT172 (Cole et al., 1998), IFT20, IFT46 (Hou et al., 2007), IFT70 (Fan et al., 2010), IFT56 (Ishikawa et al., 2014), IFT74 (Qin et al., 2004) and IFT122 (Behal et al., 2012); antibodies against motility-related proteins: FAP20 (Yanagisawa et al., 2014), MBO2 (Tam and Lefebvre, 2002), RSP3 (Diener et al., 1993) and IC97 (Wirschell et al., 2009), IC138 (Hendrickson et al., 2004), IC140 (Yang and Sale, 1998), LC1 (Benashski et al., 1999); and antibody against IFT cargo BBS4 (Lechtreck et al., 2009). Anti-β-F_1-ATPase (AtpB) was purchased from Agrisera (Sweden). Anti-IC69 was from Sigma-Aldrich (USA). The primary antibodies used in this study are listed in Table S2.

The SDS-PAGE and immunoblotting assays were performed as described (Silva et al., 2012). Chemiluminescence was used to detect the primary antibodies. The intensities of the immunoblot bands were quantified by the Image Lab™ Software (Bio-Rad, California, USA).

qPCR assay

qPCR was performed using Sybr Green PCR Dye as described previously (Wood et al., 2012). The following pairs of qPCR primers were used: q*IFT57*F/q*IFT57*R, q*IFT74*F/q*IFT74*R, q*IFT140*F/q*IFT140*R, q*IFT88*F/q*IFT88*R and q*GBLP*F/q*GBLP*R (Table S1). Primers for *IFT57* gene were designed for this study. The remaining primers were described in a previous publication (Wood et al., 2012). The guanine nucleotide-binding protein subunit β-like protein (GBLP) was used as an internal control. The program used for amplification is: 94°C for 2 min, 40 cycles of 94°C for 10 s and 60°C for 30 s, then 60°C for 2 min, finishing with a melting curve.

Photoaccumulation assay

Since most cells in *ift57-1* liquid culture were in clumps, we used the following procedure to get rid of bald cells or cell clumps before performing photoaccumulation assays (DiPetrillo and Smith, 2011). The *cc125* and *ift57-1* cells from fresh TAP plates were transferred to M1 liquid medium (Sager and Granick, 1953) and cultured with aeration for 3 days. Then flasks were left to stand still for 10 min to allow bald cells or clumps to sediment to the bottom of the flask. The upper layers were transferred to new flasks with fresh M1 media. After culturing for 2 more days, 20 ml of *cc125* and *ift57-1* cells were transferred to Petri dishes for photoaccumulation assays. Half of each Petri dish was covered by foil. The light was then shed from open sides of the dishes for 20 min. One sample was taken from the side close to the light from each dish (site 1 from *cc125*; site 3 from *ift57-1*), and one sample was taken from the side away from the light (site 2 from *cc125*; site 4 from

ift57-1). 300 randomly picked cells were analyzed for flagellar assembly from sample 1, 3 and 4; however, there were almost no cells recovered in sample 2 since almost all cells went to site 1.

Flagella isolation

Flagella were isolated as previously described (Cole et al., 1998). Briefly, cells cultured in TAP medium were deflagellated by pH shock, and then cell bodies were removed by centrifugation through a 25% sucrose cushion at 1800 rpm (652 ***g***). Isolated flagella were collected at 10,000 rpm (17,050 ***g***) in an SW 32 Ti motor (Beckman Coulter, USA). Owing to the presence of cell clumps in *ift57-1*, cells were treated with gametic autolysin for 15–20 min to dissociate clumps followed by 4 h incubation in 10 mM HEPES to encourage flagellation before flagella isolation.

Cycloheximide treatment

Chlamydomonas cells were cultured to dark green before cycloheximide (12.5 µg ml^{-1}) treatments. Protein samples were prepared at 0 h, 6 h and 12 h after adding cycloheximide.

Whole-cell sucrose density gradient

The sucrose density gradient centrifugation of whole-cell extracts was prepared the same way as described previously (Richey and Qin, 2012). The Optima XE-90 Ultracentrifuge (Beckman Coulter, USA) with an SW41 rotor was used. *Cw92*, a cell-wall-deficient mutant in the *cc125* background, was used as a wild-type control. Fractions at 19S, 12S and 10S were estimated by the sedimentation positions of Rubisco, RSP3 and FLA10, respectively.

Imaging

Flagellar assembly status analysis and length measurements

C. reinhardtii cells were fixed with 2% glutaraldehyde. Images were collected on an Axioplan phase–contrast microscope (Carl Zeiss, Oberkochen, Germany) using a 63×1.40 NA oil Plan-Apochromat objective (Olympus, Tokyo, Japan). Measurement of flagellar length was performed using ImageJ (NIH).

Assessment of flagellar waveform pattern

C. reinhardtii cells were placed in a hand-made swimming chamber of ∼100 µm thickness, and were observed under an Axioplan phase-contrast microscope with a 63×1.40 NA oil Plan-Apochromat lens. Movies were taken with a Phantom High Speed Micro-eX2 camera (Vision Research) at 600 frames per second (fps) and processed using the Cine Viewer software [version 2.6, Vision Research Inc, Prince Edward Island (P.E.I.), Canada]. Movies were imported to ImageJ for analysis.

Recording of cell-swimming tracks

Cells were cultured in M1 medium with aeration. After removing bald and cell clumps, flagellated cells were placed in chambers as described above and observed through a dark-field microscope. Tracks of swimming cells were taken with a 2 s exposures and processed in ImageJ.

TIRF microscopy and analytical methods

The strain *ift57-1 fla3-1b::KAP-GFP* was generated by crossing *ift57-1* with the strain *fla3-1b::KAP-GFP* (Mueller et al., 2005). The cross progenies were selected by phenotypes, PCR and fluorescence microscopy. The PCRs were performed using an *IFT57*-specific primer *IFT57*-51-69-F and a primer named pHyg3-624-643-R (Table S1) based on the sequence of *pHyg3*. The *fla3-1b*::KAP-GFP and *fla3-1bift57-1*::KAP-GFP cells were first cultured in TAP and then transferred to M1 liquid medium with aeration to encourage flagellar assembly. Only the cells with near full-length flagella were used for microscopic observation. The cells were immobilized in M1 medium supplemented with 10 mM Hepes (pH 7) and 6.25 mM EGTA (Wren et al., 2013). To record the motility of KAP–GFP, images were taken with an inverted Nikon eclipse-Ti microscope (Tokyo, Japan) with a 100×1.49 NA TIRF objective. Microscopic images and time-lapses were captured using a Hamamatsu ImagEM X2™ EM-CCD camera C9100-23B (Shizuoka Prefecture, Japan). The motility of KAP–GFP was imaged with a 488 nm laser under a 100× objective with 1.5× amplifier at 30 fps. The kymograph was then made using the Reslice function in ImageJ (http://rsb.info.nih.gov/ij/).

Immunofluorescence microscopy

The cell staining was carried out as previously described (Richey and Qin, 2012) with slight modifications. Briefly, cells were fixed in 100% cold methanol and then blocked in PBS containing 10% goat serum, 5% BSA, and 1% cold-water fish gelatin. Then slides were incubated with primary antibodies for 4 h at room temperature, followed by 3 washes with PBS. Slides were then incubated with secondary antibodies for 1 h at room temperature. Images were taken on an Olympus IX81 microscope (Olympus, Tokyo, Japan) with a Yokogawa CSU-X1 Spinning Disk Unit (Andor Technology, CT, USA).

Statistical analysis

Statistical analyses were performed using the software GraphPad Prism (GraphPad Software, San Diego, California, USA). Quantitative data is presented as the mean±s.d. Statistical analysis between two groups was performed with a Student's *t*-test (**P*<0.05; ***P*<0.01; ****P*<0.001; ns, represents no significant difference).

Acknowledgements

We thank Dr Wirschell at the University of Mississippi Medical Center, Cole at University of Idaho, and Dr Witman at the University of Massachusetts Medical School for kindly providing antibodies used in this study. We thank Dr Garcia at TAMU for sharing his confocal microscope for imaging. We thank the Laboratory of Biological Mass Spectrometry at TAMU for protein sequencing. We are grateful to Dr Diener at Yale and other members of the Qin laboratory for their assistance.

Competing interests

The authors declare no competing or financial interests.

Author contributions

H.Q. and X.J. conceived and designed the study, and wrote the manuscript. C.H. is responsible for Fig. 1A,E. B.N. and Z.D. helped with the TIRF microscope experiment (Fig. 6D,E). H.Q. provided results for Fig. 5A–D. K.A. assisted in recording cell motility. X.J. and D.H. performed experiments for all other figures. All authors read and approved the manuscript.

Funding

This study was supported by the Division of Molecular and Cellular Biosciences, National Science Foundation (NSF) (grant MCB-0923835 to H.Q.)

Supplementary information

Supplementary information available online at
http://jcs.biologists.org/lookup/doi/10.1242/jcs.199117.supplemental

References

Ahmed, N. T., Gao, C., Lucker, B. F., Cole, D. G. and Mitchell, D. R. (2008). ODA16 aids axonemal outer row dynein assembly through an interaction with the intraflagellar transport machinery. *J. Cell Biol.* **183**, 313-322.

Badano, J. L., Mitsuma, N., Beales, P. L. and Katsanis, N. (2006). The ciliopathies: an emerging class of human genetic disorders. *Annu. Rev. Genomics Hum. Genet.* **7**, 125-148.

Baker, S. A., Freeman, K., Luby-Phelps, K., Pazour, G. J. and Besharse, J. C. (2003). IFT20 links kinesin II with a mammalian intraflagellar transport complex that is conserved in motile flagella and sensory cilia. *J. Biol. Chem.* **278**, 34211-34218.

Behal, R. H., Miller, M. S., Qin, H., Lucker, B. F., Jones, A. and Cole, D. G. (2012). Subunit interactions and organization of the Chlamydomonas reinhardtii intraflagellar transport complex A proteins. *J. Biol. Chem.* **287**, 11689-11703.

Benashski, S. E., Patel-King, R. S. and King, S. M. (1999). Light chain 1 from the Chlamydomonas outer dynein arm is a leucine-rich repeat protein associated with the motor domain of the gamma heavy chain. *Biochemistry* **38**, 7253-7264.

Bhogaraju, S., Cajanek, L., Fort, C., Blisnick, T., Weber, K., Taschner, M., Mizuno, N., Lamla, S., Bastin, P., Nigg, E. A. et al. (2013a). Molecular basis of tubulin transport within the cilium by IFT74 and IFT81. *Science* **341**, 1009-1012.

Bhogaraju, S., Engel, B. D. and Lorentzen, E. (2013b). Intraflagellar transport complex structure and cargo interactions. *Cilia* **2**, 10.

Bower, R., VanderWaal, K., O'Toole, E., Fox, L., Perrone, C., Mueller, J., Wirschell, M., Kamiya, R., Sale, W. S. and Porter, M. E. (2009). IC138 defines a

subdomain at the base of the I1 dynein that regulates microtubule sliding and flagellar motility. *Mol. Biol. Cell* **20**, 3055-3063.
Cao, Y., Park, A. and Sun, Z. (2010). Intraflagellar transport proteins are essential for cilia formation and for planar cell polarity. *J. Am. Soc. Nephrol.* **21**, 1326-1333.
Cole, D. G., Diener, D. R., Himelblau, A. L., Beech, P. L., Fuster, J. C. and Rosenbaum, J. L. (1998). Chlamydomonas kinesin-II-dependent intraflagellar transport (IFT): IFT particles contain proteins required for ciliary assembly in Caenorhabditis elegans sensory neurons. *J. Cell Biol.* **141**, 993-1008.
Deane, J. A., Cole, D. G., Seeley, E. S., Diener, D. R. and Rosenbaum, J. L. (2001). Localization of intraflagellar transport protein IFT52 identifies basal body transitional fibers as the docking site for IFT particles. *Curr. Biol.* **11**, 1586-1590.
Diener, D. R., Ang, L. H. and Rosenbaum, J. L. (1993). Assembly of flagellar radial spoke proteins in Chlamydomonas: identification of the axoneme binding domain of radial spoke protein 3. *J. Cell Biol.* **123**, 183-190.
DiPetrillo, C. G. and Smith, E. F. (2011). The Pcdp1 complex coordinates the activity of dynein isoforms to produce wild-type ciliary motility. *Mol. Biol. Cell* **22**, 4527-4538.
Eguether, T., San Agustin, J. T., Keady, B. T., Jonassen, J. A., Liang, Y., Francis, R., Tobita, K., Johnson, C. A., Abdelhamed, Z. A., Lo, C. W. et al. (2014). IFT27 links the BBSome to IFT for maintenance of the ciliary signaling compartment. *Dev. Cell* **31**, 279-290.
Engel, B. D., Lechtreck, K.-F., Sakai, T., Ikebe, M., Witman, G. B. and Marshall, W. F. (2009a). Total internal reflection fluorescence (TIRF) microscopy of Chlamydomonas flagella. *Methods Cell Biol.* **93**, 157-177.
Engel, B. D., Ludington, W. B. and Marshall, W. F. (2009b). Intraflagellar transport particle size scales inversely with flagellar length: revisiting the balance-point length control model. *J. Cell Biol.* **187**, 81-89.
Fan, Z.-C., Behal, R. H., Geimer, S., Wang, Z., Williamson, S. M., Zhang, H., Cole, D. G. and Qin, H. (2010). Chlamydomonas IFT70/CrDYF-1 is a core component of IFT particle complex B and is required for flagellar assembly. *Mol. Biol. Cell* **21**, 2696-2706.
Gao, C., Wang, G., Amack, J. D. and Mitchell, D. R. (2010). Oda16/Wdr69 is essential for axonemal dynein assembly and ciliary motility during zebrafish embryogenesis. *Dev. Dyn.* **239**, 2190-2197.
Haycraft, C. J., Schafer, J. C., Zhang, Q., Taulman, P. D. and Yoder, B. K. (2003). Identification of CHE-13, a novel intraflagellar transport protein required for cilia formation. *Exp. Cell Res.* **284**, 249-261.
Hendrickson, T. W., Perrone, C. A., Griffin, P., Wuichet, K., Mueller, J., Yang, P., Porter, M. E. and Sale, W. S. (2004). IC138 is a WD-repeat dynein intermediate chain required for light chain assembly and regulation of flagellar bending. *Mol. Biol. Cell* **15**, 5431-5442.
Hou, Y., Qin, H., Follit, J. A., Pazour, G. J., Rosenbaum, J. L. and Witman, G. B. (2007). Functional analysis of an individual IFT protein: IFT46 is required for transport of outer dynein arms into flagella. *J. Cell Biol.* **176**, 653-665.
Houde, C., Dickinson, R. J., Houtzager, V. M., Cullum, R., Montpetit, R., Metzler, M., Simpson, E. M., Roy, S., Hayden, M. R., Hoodless, P. A. et al. (2006). Hippi is essential for node cilia assembly and Sonic hedgehog signaling. *Dev. Biol.* **300**, 523-533.
Ishikawa, H. and Marshall, W. F. (2011). Ciliogenesis: building the cell's antenna. *Nat. Rev. Mol. Cell Biol.* **12**, 222-234.
Ishikawa, H., Ide, T., Yagi, T., Jiang, X., Hirono, M., Sasaki, H., Yanagisawa, H., Wemmer, K. A., Stainier, D. Y., Qin, H. et al. (2014). TTC26/DYF13 is an intraflagellar transport protein required for transport of motility-related proteins into flagella. *Elife* **3**, e01566.
Katoh, Y., Terada, M., Nishijima, Y., Takei, R., Nozaki, S., Hamada, H. and Nakayama, K. (2016). Overall architecture of the Intraflagellar Transport (IFT)-B complex containing Cluap1/IFT38 as an essential component of the IFT-B peripheral subcomplex. *J. Biol. Chem.* **291**, 10962-10975.
King, S. M. (2012). Integrated control of axonemal dynein AAA(+) motors. *J. Struct. Biol.* **179**, 222-228.
Kozminski, K. G., Beech, P. L. and Rosenbaum, J. L. (1995). The Chlamydomonas kinesin-like protein FLA10 is involved in motility associated with the flagellar membrane. *J. Cell Biol.* **131**, 1517-1527.
Krock, B. L. and Perkins, B. D. (2008). The intraflagellar transport protein IFT57 is required for cilia maintenance and regulates IFT-particle-kinesin-II dissociation in vertebrate photoreceptors. *J. Cell Sci.* **121**, 1907-1915.
Kubo, T., Kaida, S., Abe, J., Saito, T., Fukuzawa, H. and Matsuda, Y. (2009). The Chlamydomonas hatching enzyme, sporangin, is expressed in specific phases of the cell cycle and is localized to the flagella of daughter cells within the sporangial cell wall. *Plant Cell Physiol.* **50**, 572-583.
Kubo, T., Brown, J. M., Bellve, K., Craige, B., Craft, J. M., Fogarty, K., Lechtreck, K. F. and Witman, G. B. (2016). Together, the IFT81 and IFT74 N-termini form the main module for intraflagellar transport of tubulin. *J. Cell Sci.* **129**, 2106-2119.
Lechtreck, K. F. (2015). IFT-Cargo interactions and protein transport in Cilia. *Trends Biochem. Sci.* **40**, 765-778.
Lechtreck, K.-F., Johnson, E. C., Sakai, T., Cochran, D., Ballif, B. A., Rush, J., Pazour, G. J., Ikebe, M. and Witman, G. B. (2009). The Chlamydomonas reinhardtii BBSome is an IFT cargo required for export of specific signaling proteins from flagella. *J. Cell Biol.* **187**, 1117-1132.
Lucker, B. F., Behal, R. H., Qin, H., Siron, L. C., Taggart, W. D., Rosenbaum, J. L. and Cole, D. G. (2005). Characterization of the intraflagellar transport complex B core: direct interaction of the IFT81 and IFT74/72 subunits. *J. Biol. Chem.* **280**, 27688-27696.
Mueller, J., Perrone, C. A., Bower, R., Cole, D. G. and Porter, M. E. (2005). The FLA3 KAP subunit is required for localization of kinesin-2 to the site of flagellar assembly and processive anterograde intraflagellar transport. *Mol. Biol. Cell* **16**, 1341-1354.
Mukhopadhyay, S., Wen, X., Chih, B., Nelson, C. D., Lane, W. S., Scales, S. J. and Jackson, P. K. (2010). TULP3 bridges the IFT-A complex and membrane phosphoinositides to promote trafficking of G protein-coupled receptors into primary cilia. *Genes Dev.* **24**, 2180-2193.
Pazour, G. J., Wilkerson, C. G. and Witman, G. B. (1998). A dynein light chain is essential for the retrograde particle movement of intraflagellar transport (IFT). *J. Cell Biol.* **141**, 979-992.
Pazour, G. J., Dickert, B. L. and Witman, G. B. (1999). The DHC1b (DHC2) isoform of cytoplasmic dynein is required for flagellar assembly. *J. Cell Biol.* **144**, 473-481.
Pazour, G. J., Agrin, N., Leszyk, J. and Witman, G. B. (2005). Proteomic analysis of a eukaryotic cilium. *J. Cell Biol.* **170**, 103-113.
Perkins, L. A., Hedgecock, E. M., Thomson, J. N. and Culotti, J. G. (1986). Mutant sensory cilia in the nematode Caenorhabditis elegans. *Dev. Biol.* **117**, 456-487.
Perrone, C. A., Yang, P., O'Toole, E., Sale, W. S. and Porter, M. E. (1998). The Chlamydomonas IDA7 locus encodes a 140-kDa dynein intermediate chain required to assemble the I1 inner arm complex. *Mol. Biol. Cell* **9**, 3351-3365.
Pigino, G., Geimer, S., Lanzavecchia, S., Paccagnini, E., Cantele, F., Diener, D. R., Rosenbaum, J. L. and Lupetti, P. (2009). Electron-tomographic analysis of intraflagellar transport particle trains in situ. *J. Cell Biol.* **187**, 135-148.
Pollock, S. V., Prout, D. L., Godfrey, A. C., Lemaire, S. D. and Moroney, J. V. (2004). The Chlamydomonas reinhardtii proteins Ccp1 and Ccp2 are required for long-term growth, but are not necessary for efficient photosynthesis, in a low-CO2 environment. *Plant Mol. Biol.* **56**, 125-132.
Porter, M. E., Bower, R., Knott, J. A., Byrd, P. and Dentler, W. (1999). Cytoplasmic dynein heavy chain 1b is required for flagellar assembly in Chlamydomonas. *Mol. Biol. Cell* **10**, 693-712.
Qin, H., Diener, D. R., Geimer, S., Cole, D. G. and Rosenbaum, J. L. (2004). Intraflagellar transport (IFT) cargo: IFT transports flagellar precursors to the tip and turnover products to the cell body. *J. Cell Biol.* **164**, 255-266.
Richey, E. A. and Qin, H. (2012). Dissecting the sequential assembly and localization of intraflagellar transport particle complex B in Chlamydomonas. *PLoS ONE* **7**, e43118.
Rosenbaum, J. L. and Witman, G. B. (2002). Intraflagellar transport. *Nat. Rev. Mol. Cell Biol.* **3**, 813-825.
Sager, R. and Granick, S. (1953). Nutritional studies with Chlamydomonas reinhardi. *Ann. N. Y. Acad. Sci.* **56**, 831-838.
Silva, D. A., Huang, X., Behal, R. H., Cole, D. G. and Qin, H. (2012). The RABL5 homolog IFT22 regulates the cellular pool size and the amount of IFT particles partitioned to the flagellar compartment in Chlamydomonas reinhardtii. *Cytoskeleton* **69**, 33-48.
Tam, L.-W. and Lefebvre, P. A. (2002). The Chlamydomonas MBO2 locus encodes a conserved coiled-coil protein important for flagellar waveform conversion. *Cell Motil. Cytoskeleton* **51**, 197-212.
Taschner, M., Bhogaraju, S., Vetter, M., Morawetz, M. and Lorentzen, E. (2011). Biochemical mapping of interactions within the intraflagellar transport (IFT) B core complex: IFT52 binds directly to four other IFT-B subunits. *J. Biol. Chem.* **286**, 26344-26352.
Taschner, M., Kotsis, F., Braeuer, P., Kuehn, E. W. and Lorentzen, E. (2014). Crystal structures of IFT70/52 and IFT52/46 provide insight into intraflagellar transport B core complex assembly. *J. Cell Biol.* **207**, 269-282.
Taschner, M., Weber, K., Mourão, A., Vetter, M., Awasthi, M., Stiegler, M., Bhogaraju, S. and Lorentzen, E. (2016). Intraflagellar transport proteins 172, 80, 57, 54, 38, and 20 form a stable tubulin-binding IFT-B2 complex. *EMBO J.* **35**, 773-790.
Viswanadha, R., Hunter, E. L., Yamamoto, R., Wirschell, M., Alford, L. M., Dutcher, S. K. and Sale, W. S. (2014). The ciliary inner dynein arm, I1 dynein, is assembled in the cytoplasm and transported by IFT before axonemal docking. *Cytoskeleton* **71**, 573-586.
Walther, Z., Vashishtha, M. and Hall, J. L. (1994). The Chlamydomonas FLA10 gene encodes a novel kinesin-homologous protein. *J. Cell Biol.* **126**, 175-188.
Wirschell, M., Yang, C., Yang, P., Fox, L., Yanagisawa, H.-A., Kamiya, R., Witman, G. B., Porter, M. E. and Sale, W. S. (2009). IC97 is a novel intermediate chain of I1 dynein that interacts with tubulin and regulates interdoublet sliding. *Mol. Biol. Cell* **20**, 3044-3054.
Wood, C. R., Wang, Z., Diener, D., Zones, J. M., Rosenbaum, J. and Umen, J. G. (2012). IFT proteins accumulate during cell division and localize to the cleavage furrow in Chlamydomonas. *PLoS ONE* **7**, e30729.
Wren, K. N., Craft, J. M., Tritschler, D., Schauer, A., Patel, D. K., Smith, E. F., Porter, M. E., Kner, P. and Lechtreck, K. F. (2013). A differential

Journal of Cell Science

cargo-loading model of ciliary length regulation by IFT. *Curr. Biol.* **23**, 2463-2471.

Yanagisawa, H.-A., Mathis, G., Oda, T., Hirono, M., Richey, E. A., Ishikawa, H., Marshall, W. F., Kikkawa, M. and Qin, H. (2014). FAP20 is an inner junction protein of doublet microtubules essential for both the planar asymmetrical waveform and stability of flagella in Chlamydomonas. *Mol. Biol. Cell* **25**, 1472-1483.

Yang, P. and Sale, W. S. (1998). The Mr 140,000 intermediate chain of Chlamydomonas flagellar inner arm dynein is a WD-repeat protein implicated in dynein arm anchoring. *Mol. Biol. Cell* **9**, 3335-3349.

Yang, P., Diener, D. R., Yang, C., Kohno, T., Pazour, G. J., Dienes, J. M., Agrin, N. S., King, S. M., Sale, W. S., Kamiya, R. et al. (2006). Radial spoke proteins of Chlamydomonas flagella. *J. Cell Sci.* **119**, 1165-1174.